Discovery of a Highly Variable Dipping Ultraluminous X-Ray Source in M94

Dacheng Lin – University of Alabama

Jimmy A. Irwin – University of Alabama

Natalie A. Webb – Université de Toulouse

Didier Barret – Université de Toulouse

Ronald A. Remillard – MIT Kavli Institute

Citation of published version:

Lin, D., Irwin, J., Webb, N., Barret, D., Remillard, R. (2013): Discovery of a Highly Variable Dipping Ultraluminous X-Ray Source in M94. *The Astrophysical Journal*, 779(2). http://dx.doi.org/10.1088/0004-637X/779/2/149

The Astrophysical Journal, 779:149 (9pp), 2013 December 20 doi:10.1088/0004-637X/779/2/149

DISCOVERY OF A HIGHLY VARIABLE DIPPING ULTRALUMINOUS X-RAY SOURCE IN M94

Dacheng Lin[1,2,3], Jimmy A. Irwin[1], Natalie A. Webb[2,3], Didier Barret[2,3], and Ronald A. Remillard[4]
[1] Department of Physics and Astronomy, University of Alabama, Box 870324, Tuscaloosa, AL 35487, USA; dlin@ua.edu
[2] CNRS, IRAP, 9 avenue du Colonel Roche, BP 44346, F-31028 Toulouse Cedex 4, France
[3] Université de Toulouse, UPS-OMP, IRAP, Toulouse, France
[4] MIT Kavli Institute for Astrophysics and Space Research, MIT, 70 Vassar Street, Cambridge, MA 02139-4307, USA
Received 2013 July 8; accepted 2013 October 31; published 2013 December 3

ABSTRACT

We report the discovery of a new ultraluminous X-ray source (ULX) 2XMM J125048.6+410743 within the spiral galaxy M94. The source has been observed by *ROSAT*, *Chandra*, and *XMM-Newton* on several occasions, exhibiting as a highly variable persistent source or a recurrent transient with a flux variation factor of $\gtrsim$100, a high duty cycle (at least ∼70%), and a peak luminosity of $L_X \sim 2 \times 10^{39}$ erg s^{-1} (0.2–10 keV, absorbed). In the brightest observation, the source is similar to typical low-luminosity ULXs, with the spectrum showing a high-energy cutoff but harder than that from a standard accretion disk. There are also sporadical short dips, accompanied by spectral softening. In a fainter observation with $L_X \sim 3.6 \times 10^{38}$ erg s^{-1}, the source appears softer and is probably in the thermal state seen in Galactic black hole X-ray binaries (BHBs). In an even fainter observation ($L_X \sim 9 \times 10^{37}$ erg s^{-1}), the spectrum is harder again, and the source might be in the steep-power-law state or the hard state of BHBs. In this observation, the light curve might exhibit ∼7 hr (quasi-)periodic large modulations over two cycles. The source also has a possible point-like optical counterpart from *Hubble Space Telescope* images. In terms of the colors and the luminosity, the counterpart is probably a G8 supergiant or a compact red globular cluster containing $\sim 2 \times 10^5$ K dwarfs, with some possible weak UV excess that might be ascribed to accretion activity. Thus, our source is a candidate stellar-mass BHB with a supergiant companion or with a dwarf companion residing in a globular cluster. Our study supports that some low-luminosity ULXs are supercritically accreting stellar-mass BHBs.

Key words: accretion, accretion disks – black hole physics – X-rays: binaries – X-rays: individual: 2XMM J125048.6+410743

Online-only material: color figures

1. INTRODUCTION

Many bright X-ray sources have been discovered in nearby galaxies. Those with luminosities L_X exceeding 10^{39} erg s^{-1}, the Eddington limit for a black hole X-ray binary (BHB) with a black hole (BH) mass of $M_{BH} \sim 10\,M_\odot$, are often referred to as ultraluminous X-ray sources (ULXs; for a recent review, see Feng & Soria 2011), while a very small number of them appear as hyperluminous X-ray sources (HLXs; especially ESO 243-49 HLX-1) with $L_X > 10^{41}$ erg s^{-1} and are strong candidates for intermediate-mass BHs (IMBHs) with $M_{BH} \sim 10^2$–$10^5\,M_\odot$ (Farrell et al. 2009; Jonker et al. 2010; Servillat et al. 2011; Sutton et al. 2012; Godet et al. 2012), most ULXs have $L_X < 10^{40}$ erg s^{-1}. The nature of these "low-luminosity" ULXs is still under strong debate. They could be IMBHs (e.g., Colbert & Mushotzky 1999), super-Eddington low-mass BHs (e.g., Komossa & Schulz 1998), beamed emission from geometrically thick disks at high accretion rates (King et al. 2001) or from relativistic jets (Okada et al. 1998), or a combination of these effects (Poutanen et al. 2007; King 2009).

Due to their large distances, there are no confident dynamical mass measurements for ULXs yet (Feng & Soria 2011), unlike Galactic BHBs, whose dynamical masses of the BHs are constrained to below $20\,M_\odot$ (Remillard & McClintock 2006). The spectral and timing properties of Galactic BHBs have been well studied, and they are known to exhibit three characteristic X-ray spectral states: the thermal state has a dominant thermal disk and weak fast variability, typically at luminosities above a few percent of the Eddington limit; the hard state has a dominant hard power law (PL; with photon index Γ_{PL} typically within 1.4–2.1) and strong fast variability, generally seen at low luminosities; and the steep-PL state has a powerful PL with $\Gamma_{PL} \sim 2.5$ and commonly occurring quasi-periodic oscillations, often seen at very high luminosities (Remillard & McClintock 2006; McClintock & Remillard 2006; Done et al. 2007). These states also often show correlated radio emission (Fender et al. 2004). Thus, studies of ULXs often compare their properties with those of Galactic BHBs to infer their possible nature.

Two transient ULXs were discovered in M31 recently (Middleton et al. 2012, 2013). When they reached luminosities above 10^{39} erg s^{-1}, their X-ray spectra appeared harder than those from a standard geometrically thin optically thick disk. This is often seen in low-luminosity ULXs, and one possible explanation is Compton upscattering of disk photons in a wind or photosphere (Middleton et al. 2012, 2013). The above similarity led Middleton et al. (2012, 2013) to conclude that these two transient ULXs in M31 are members of low-luminosity ULXs, though the latter are mostly persistent with small long-term variability (Feng & Soria 2011). However, these two ULXs are also similar to BHBs with stellar-mass BHs in other aspects, such as the outburst profile and the coupled X-ray and radio behavior. Thus, Middleton et al. (2012, 2013) concluded that many low-luminosity ULXs are stellar-mass BHBs.

In Lin et al. (2012b), we classified 4330 sources from the 2XMMi-DR3 catalog (Watson et al. 2009). In this project, many sources showing interesting behavior but poorly studied in the literature were also discovered. We are devoting a series of papers (e.g., Lin et al. 2011, 2013a, 2013b) to presenting the properties of these sources in detail. Here we continue our study and concentrate on a highly variable ULX 2XMM J125048.6+410743 in the spiral galaxy M94 (NGC 4736), which shows some evidence of dips, periodic

Table 1
The X-Ray Observation Log

Obs. ID (1)	Date (2)	Detector (3)	OAA (4)	T (ks) (5)	r_{src} (6)	S/N (7)
XMM-Newton						
0094360601(X1)	2002 May 23	pn/M1/M2	2.′3	15/20/20	15″	5
0094360701(X2)	2002 Jun 26	pn/M1/M2	2.′5	4/12/12	15″	5
0404980101(X3)	2006 Nov 28	pn/M1/M2	1.′6	34/46/46	15″	112
Chandra						
808(C1)	2000 May 13	ACIS-S3	0.′8	47	1.″5	17
9553(C2)	2008 Feb 16	ACIS-I2	0.′5	24	1.″5	18
ROSAT						
RP600050N00(R1)	1991 Jun 5	PSPCB	1.′2	91	20″	32
RH600678N00(R2)	1994 Dec 7	HRI	0.′9	112	7″	1
RH600769N00(R3)	1994 Dec 25	HRI	0.′9	27	7″	0

Notes. Columns: (1) the observation ID with our designation given in parentheses, (2) the observation start date, (3) the detector, (4) the off-axis angle, (5) the exposures of data used in final analysis, (6) radius of the source extraction region, (7) the signal-to-noise ratio of the source, combining all detectors.

oscillations, and a state transition and has a possible optical counterpart from the *Hubble Space Telescope* (*HST*) images. The source, whose 1σ positional error is 0.″35 per coordinate from the 2XMMi-DR3 catalog, is only 0.″26 away from CXO J125048.6+410742 (R.A. = $12^h50^m48^s.605$, decl. = $+41^d07'42''.35$, and the 95% error is 0.″29) in the Chandra Source Catalog (CSC, release 1.1; Evans et al. 2010). Thus, we conclude that they are the same source. It should also be the off-nuclear source detected in a *ROSAT*/PSPCB observation in Cui et al. (1997), because they coincide within 5″ in position and there are no other bright sources within 20″ from *Chandra* observations. We designate the source as ULX2 hereafter, considering that there is a different ULX (U30 in Berghea et al. 2008), which is hardly variable and has a flux comparable to the peak value of our source. In Section 2, we describe the analysis of X-ray and optical observations. In Section 3, we present the results. In Section 4, we discuss the nature of the source and the cause of its short-term X-ray variability. The conclusions of our studies are given in Section 5. Throughout the paper, we assume a source distance of 5.2 Mpc (Tonry et al. 2001).

2. DATA ANALYSIS

2.1. X-Ray Observations

M94 has been observed by many X-ray observatories. However, because ULX2 is faint and is only 1′ away from the nucleus around which there are strong diffuse emission and many bright point sources, including the low-ionization nuclear emission-line region (LINER) nucleus, we only studied the eight observations (Table 1) from *XMM-Newton*, *Chandra*, and *ROSAT*, thanks to their relatively large effective areas and high angular resolutions. We designate their observations as X1-X3, C1-C2, and R1-R3, respectively (refer to Table 2). In the *XMM-Newton* observations, all three European Photon Imaging Cameras, i.e., pn, MOS1 (or M1), and MOS2 (or M2) (Jansen et al. 2001; Strüder et al. 2001; Turner et al. 2001), were active. We used SAS 12.0.1 and the calibration files of 2013 January for reprocessing the X-ray event files and follow-up analysis. The data in strong background flare intervals are excluded following the SAS thread for the filtering against high backgrounds. The event selection criteria followed the default values in the pipeline (see Table 5 in Watson et al. 2009). That is, for pn spectra, we used events with PATTERN $\leqslant$4 and FLAG = 0 (we also extracted pn light curves, which used events with (FLAG & 0xffffffef) = 0), and for MOS spectra, we used events with PATTERN $\leqslant$12 and (FLAG & 0xffffffeff) = 0. The two *Chandra* observations used the imaging array of the AXAF CCD Imaging Spectrometer (ACIS; Bautz et al. 1998). ULX2 falls in the back-illuminated chip S3 and the front-illuminated chip I2 in observations C1 and C2, respectively. We analyzed the data with the CIAO (version 4.5) package and the latest calibration (CALDB 4.5.5.1). The *ROSAT* (Truemper 1982) observations were reduced with FTOOLS 6.12.

We extracted the source emission from a circular region with the radius for each observation given in Table 1. The background in the *XMM-Newton* and *ROSAT* observations strongly depends on the distance to the nucleus due to the presence of bright sources near the nucleus and the relatively large point-spread functions (PSFs) of these two observatories, and we estimated it using four circular regions with the same radius and the same distance to the nucleus as the source region. The *Chandra* observations have no such problem thanks to their supreme angular resolutions, and we used a single circular region of 10″ radius near the source to estimate the background. We extracted both the source and background spectra/light curves from the source and background regions, respectively. The response files were constructed for the spectral fitting. We note that we took special care to construct the response file for the *ROSAT*/PSPCB observation R1. The problem is that we used a small source extraction region (a radius of 20″) in order to minimize the contamination from bright sources near the nucleus, leading to significant PSF loss, which is energy dependent. The response file (we used the default on-axis version in the HEASARC archive) does not take into account the PSF loss, and there is no FTOOLS tool to correct for this. We estimate the PSF loss using the *ROSAT* observation RP700130N00 of Mkn 501 (it used the same gain epoch and has a similar (low) column density and photon index ($\sim$2.6) as our source) and correct the count rate in each channel of the spectrum of our source. Such a correction is probably very approximate. Thus, the spectral fits to this spectrum might be subject to some systematic error due to this and will be mostly used to infer the luminosity.

We rebinned the spectra to have at least 20 counts in each bin so as to adopt the χ^2 statistic for spectral fits. All spectral models used include the absorption described by the WABS model in XSPEC, with the lower limit of N_H set to be the Galactic line-of-sight value of 10^{20} cm^{-2} (Kalberla et al. 2005).

To help to identify the optical counterpart (Section 2.2), we used X-ray sources within 2′ from the nucleus to improve the relative astrometry between *Chandra* and *HST*. To have good relative positions for these X-ray sources, we carried out the source detection using the CIAO task `wavdetect` (Freeman et al. 2002). We used only the *Chandra* observation C1 so that all sources of interest are in a single CCD, which is not the case for observation C2. We performed the detection on the 0.3–8 keV image, which was binned at a subpixel resolution (1/8 sky pixel) to improve the source positions.

2.2. HST Observations

The sky region around ULX2 was observed by the Wide Field Planetary Camera 2 (WFPC2) aboard the *HST* several times (Table 2). We aligned their drizzled images by matching the point sources to those in the F555W image, resulting

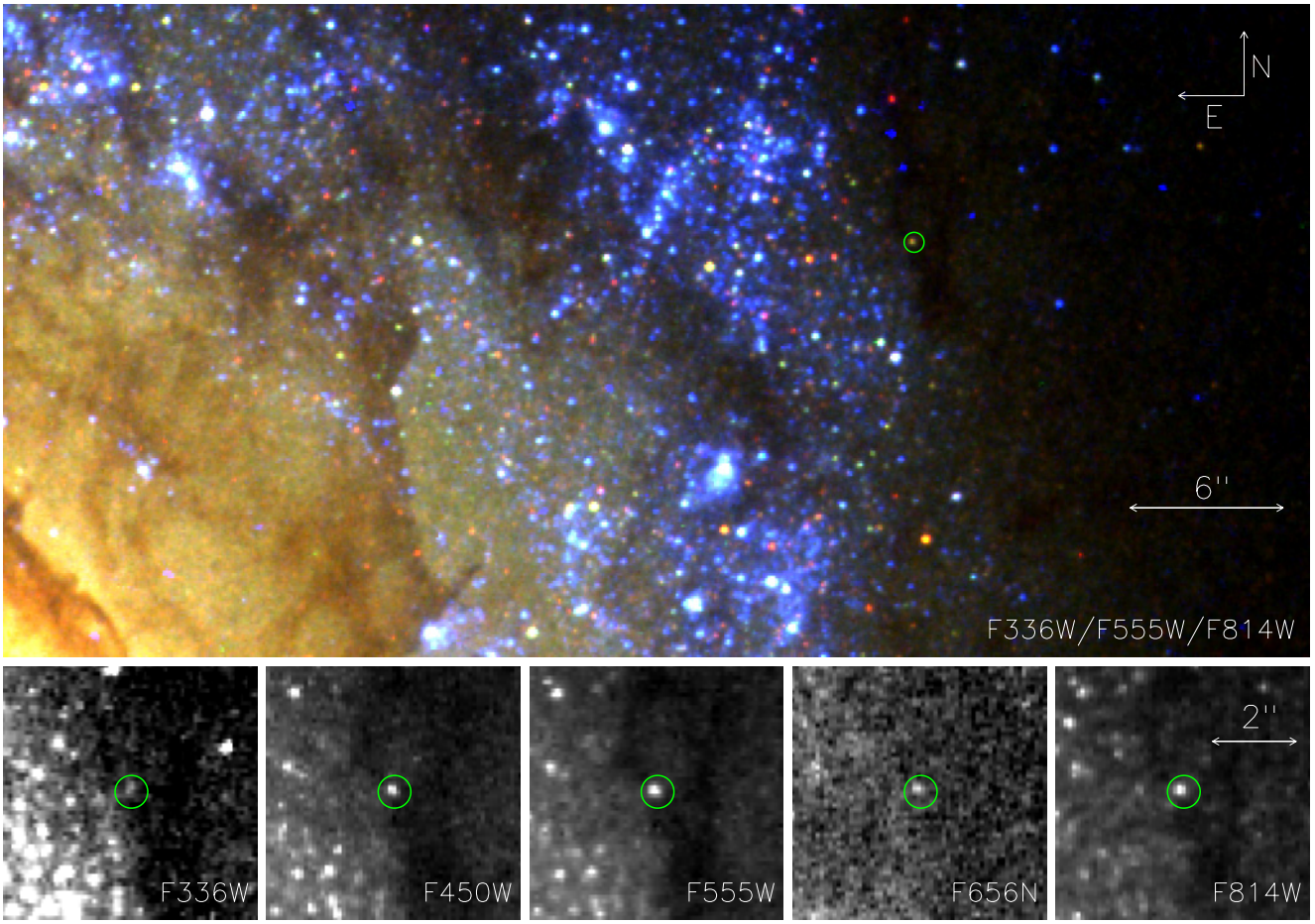

Figure 1. *HST*/WFPC2 images around ULX2. The top panel is false-colored using the F814W (red), F555W (green), and F336W (blue) images. The bottom panels, one for each of the five filters, are zoomed in on ULX2. The green circle, with a radius of 0.″39 (the 95% systematic error of *Chandra*; Rots & Budavári 2011), is centered at the X-ray position, indicating the presence of a possible optical counterpart to ULX2.

Table 2
The *HST*/WFPC2 Observation Log

Exposure ID	Date	Chip and Filter	T	S/N	VEGA mag		
			(s)		Counterpart	G8I	K3V
(1)	(2)	(3)	(4)	(5)	(6)	(7)	(8)
u96r060[1|2]m	2005 May 24	WF3/F336W	1800	6	23.18 ± 0.18	24.65	23.93
u6ea800[1r|2m]	2001 Jul 2	WF3/F450W	460	24	22.88 ± 0.05	23.05	22.96
u96r060[3|4]m	2005 May 25	WF3/F555W	400	40	22.25 ± 0.03	22.16	22.21
u671260[1-5]r	2001 Apr 21	WF2/F656N	1700	8	20.81 ± 0.13	21.13	21.20
u6ea800[3|4]r	2001 Jul 2	WF3/F814W	460	46	21.04 ± 0.02	21.07	21.05

Notes. Columns: (1) the exposure ID of the data set, (2) the observation date, (3) the chip and filter, (4) the total exposure, (5) the signal-to-noise ratio, (6) the VEGA mag of the optical counterpart to ULX2, (7 and 8) magnitudes estimated based on a G8I stellar spectrum and a K3V stellar spectrum, respectively.

in the rms deviations $<0.''04$ in all cases. To map the X-ray positions onto the *HST* images, we assumed that CXO J125053.0+410713 in the CSC and the UV source at the center of the *HST* images are the nuclear source and coincident with each other in position (see, e.g., Constantin & Seth 2012). Because the nuclear UV source is stronger and less subject to stellar contamination at shorter wavelength and thus appears more clear in the F336W image than in the other images, we used the F336W image to determine its position with the astrolib IDL procedure `cntrd`. We found that it happens to be only $0.''02$ away from the position of CXO J125053.0+410713 determined by us (Section 2.1). After correcting for this small relative astrometry, we found an optical point source that is only $0.''1$ away from ULX2 and was detected in all filters (Figure 1). We also found three other X-ray sources with optical counterpart candidates within $0.''1$, supporting our astrometry correction. We performed the photometry on the c0f images with the HSTPHOT 1.1 package (Dolphin 2000), which outputs aperture-corrected VEGA magnitudes.

3. RESULTS

3.1. Long-term X-Ray Variability

Table 1 lists the signal-to-noise ratio (S/N) of ULX2 in each observation. The source was significantly detected in observations X3, C1, C2, and R1 (S/N $\geqslant$ 17), but it

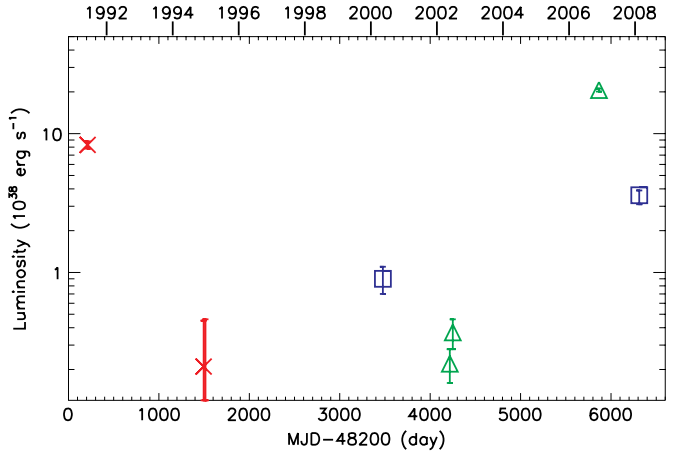

Figure 2. Long-term luminosity curve (0.2–10 keV, absorbed), with *ROSAT* (red crosses), *XMM-Newton* (green triangles), and *Chandra* (blue squares) observations. We note that the third *ROSAT* observation (R3), with $L_X = 0^{+0.46} \times 10^{38}$ erg s^{-1}, has only the error bar seen and is very close to the second one (R2, both in 1994 December).

(A color version of this figure is available in the online journal.)

was only marginally detected in observations X1 and X2 (S/N = 5) and was not detected in observations R2 and R3 (S/N $\leqslant$ 1). Figure 2 plots the long-term 0.2–10 keV absorbed luminosity curve of ULX2. The spectral models that we assumed to derive the luminosities are those shown in Figure 3 for the bright observations (X3, C1, C2, and R1) and a PL for the other faint observations, which will be described in Section 3.3. The luminosity reached $L_X \sim 2 \times 10^{39}$ erg s^{-1} in observation X3, supporting ULX2 as a low-luminosity ULX. This luminosity is a factor of $\sim$100 of that of observation X1 (we did not use observations R2 and R3 for comparison because their luminosities have larger uncertainties). Considering that observations R2 and R3 are close in time and that X1 and X2 are close in time too, ULX2 was observed in essentially six epochs and detected in four (or in five if the detections in X1 and X2 are really from ULX2) of them over nearly two decades. Thus, the source has a large duty cycle ($\sim$70% or more) and is probably a highly variable persistent source or a recurrent transient with probably at least three outbursts in the past two decades (see Figure 2). Considering that observations X3 and C2 are about 1 yr apart, the outburst should last more than 1 yr if they are in the same outburst.

3.2. Short-term X-Ray Variability

The left panels of Figure 3 show the light curves of the four observations when ULX2 was significantly detected, in order of decreasing luminosity from the top to the bottom panels. The brightest observation X3 seems to experience dipping behavior sporadically (15 ks and 25 ks into the observation), with duration a few hundred seconds. To understand the spectral properties in the dipping periods, we extracted the spectrum in the dipping period when the pn 1–10 keV count rate is <0.06 counts s^{-1} (refer to Figure 3). The spectrum turns out to be soft. When we fitted it with a multi-color disk (MCD; diskbb in XSPEC), we obtained the inner disk temperature $kT_{\rm MCD} = 0.36 \pm 0.06$ keV (the column density is $N_{\rm H} = 1^{+5} \times 10^{20}$ cm^{-2}, and the reduced χ^2 is relatively high (2.0) for six degrees of freedom (dof)). In comparison, the total spectrum gives $kT_{\rm MCD} = 0.86 \pm 0.02$ keV (Section 3.3). The hardness ratio, defined as the pn count rate in 1–10 keV, divided by that in 0.2–1 keV, is 0.31 $\pm$ 0.06 in the above dipping period, significantly lower than that (1.05 $\pm$ 0.02) from the whole observation. We also calculated the ratio of the pn count rate in the dipping period to that from the whole observation and obtained 0.78 ± 0.08 using 0.2–1 keV events and 0.23 ± 0.04 using 1–2 keV events. Thus, the dips are accompanied by spectral softening. Because of this, we created the light curve using a high-energy band (1–10 keV) for this bright observation to show the dips more clearly. Dips might also be present in the two fainter observations R1 and C2, but not clearly seen due to low counting statistics.

In contrast, the light curve of the fainter observation C1 might show three flares that could possibly indicate $\sim$7 hr (quasi-)periodic modulations over two cycles. Using a 60 ks window to calculate the count rates at different times, we found that the count rates in the three flares are about 3.3, 5.0, and 6.8 times of those in the minima (the count rates in the two minima are similar), corresponding to about 4σ, 6σ, and 7σ, respectively. We also extracted the spectra in the bright and faint intervals, depending on whether the count rate is larger or smaller than 0.005 counts s^{-1}. When we fitted them with a PL, we obtained their photon indices to be $\Gamma_{\rm PL} = 2.5 \pm 0.2$ and 2.6 ± 0.4, respectively (we fixed $N_{\rm H}$ at 6×10^{20} cm^{-2} obtained from the fit to the total spectrum (Section 3.3) because of the low counting statistics of the spectra). We also calculated the hardness ratio, defined as the count rate in 1–8 keV divided by that in 0.3–1 keV and obtained the values of 0.71 $\pm$ 0.11 and 0.76 ± 0.23 for the bright and faint intervals, respectively. Thus, we see no clear spectral variability associated with the flares in observation C1.

3.3. Spectral Modeling

The brightest observation X3 has the best quality and allows for relatively detailed modeling. Following Stobbart et al. (2006), we fitted the 2–10 keV spectrum with a PL and a broken PL (both unabsorbed) and found that the latter fit (the total χ^2 is 98.2 for 118 dof) showed a significant (5σ) improvement over the former one (the total χ^2 is 125.2 for 120 dof), indicating the presence of spectral curvature at several keV (the inferred break energy is 4.6 $\pm$ 0.7 keV). The fits over the whole spectrum (0.2–10 keV) with a PL are very poor, with a reduced χ^2 of 1.31 (560 dof, Table 3). The fit with the MCD model is better (the reduced χ^2 is 1.15), but there are still clear residuals at high energies, as is often seen in the spectral fits to ULXs and was explained as due to the advection effect and/or the Compton scattering of disk photons in an optically thick wind, photosphere, or corona in many studies, such as Gladstone et al. (2009) and Middleton et al. (2012, 2013). Similar to these studies, we tested two-component models to include a Comptonization component, i.e., MCD+PL and MCD+CompTT (CompTT (Titarchuk 1994) is available in XSPEC). The fit with the MCD+PL model is much better than that with the MCD model, decreasing the total χ^2 by 114. The MCD+CompTT model, with the seed photons tied to the inner disk temperature, decreases the total χ^2 further, by 32 compared with the MCD+PL model for one more dof. The MCD+CompTT model inferred a population of cool (1.0 keV) Comptonizing electrons with a high optical depth ($\tau \sim 11$). For the disk, we inferred $kT_{\rm MCD} = 0.25^{+0.07}_{-0.04}$ keV (90% error) or $kT_{\rm MCD} = 0.25^{+0.30}_{-0.05}$ keV (2σ error) (here we report two error bars because we found that χ^2 varied slowly for a relatively large range of $kT_{\rm MCD}$).

We also tested the Comptonization model nthComp (in XSPEC; Życki et al. 1999; Zdziarski et al. 1996; Lightman

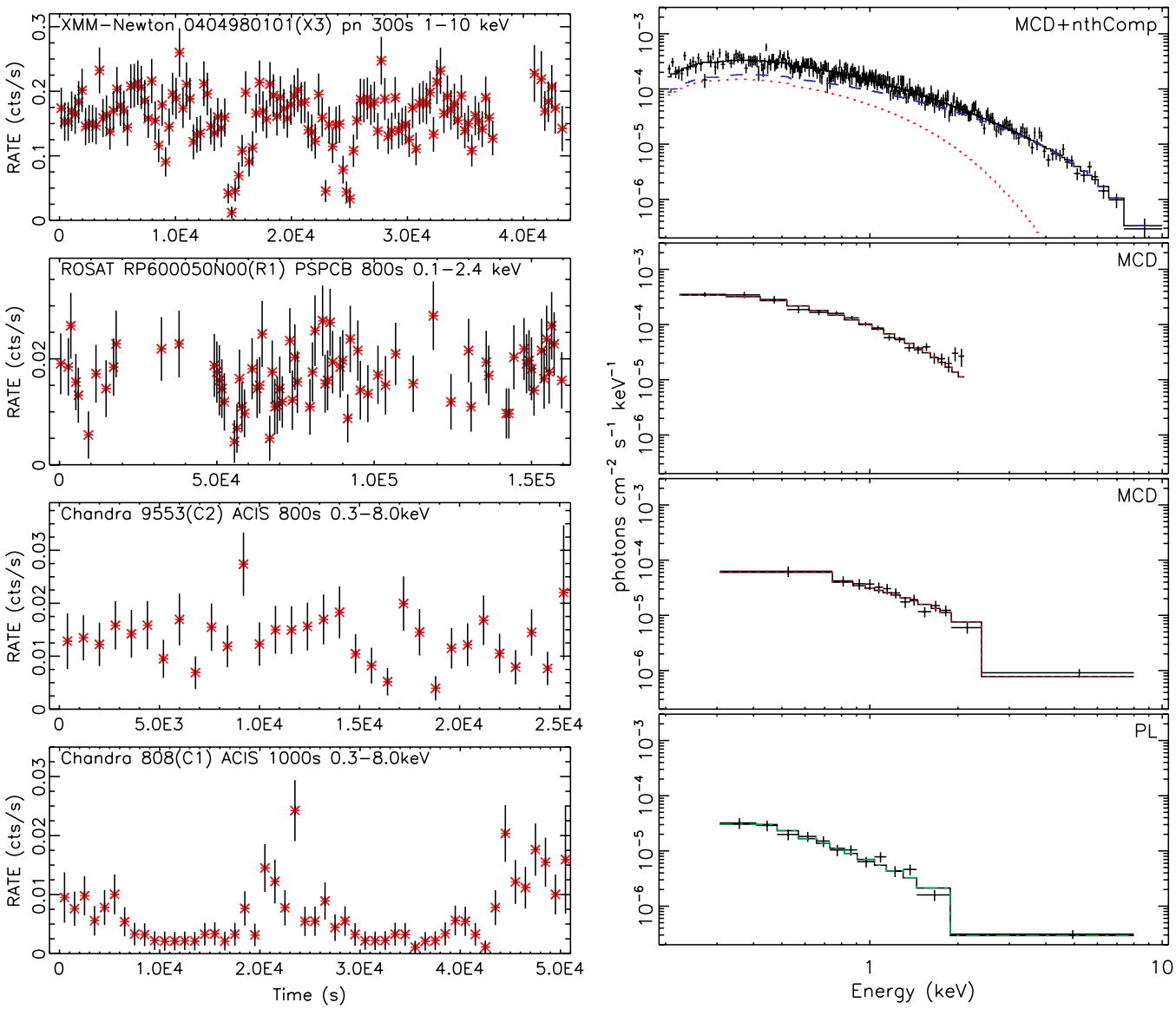

Figure 3. Light curves (left panels) and unfolded spectra (right panels) of the four observations (the luminosity decreases from the top to the bottom panels) when ULX2 was significantly detected. The notation in the left panels includes the observatory, the observation ID, the instrument, the light-curve bin size, and the energy band used, and that in the right panels is the spectral model used. The total model is shown as a black solid line, the MCD component as a red dotted line, the nthComp component as a blue dashed line, and the PL component as a green dot-dashed line.

(A color version of this figure is available in the online journal.)

& Zdziarski 1987), whose seed photons can be assumed to have the MCD shape. This model was used in the fits to very bright (around the Eddington limit) spectra from the ρ state of the BHB GRS 1915+105 by Neilsen et al. (2011) and those from the luminous neutron star (NS) low-mass X-ray binary (LMXB) GX 17+2 by Lin et al. (2012a) as a substitution of the SIMPL model (Steiner et al. 2009) to account for the high-energy cutoff in the spectra. The fitting results with the MCD+nthComp model are given in Table 3, and the unfolded spectrum is shown in Figure 3. The MCD normalization is not well constrained, with the 90% confidence lower limit reaching zero, which was also seen in Neilsen et al. (2011) and Lin et al. (2012a). Following Lin et al. (2012a), we roughly estimated the pre-Comptonization disk normalization $N_{\rm disk,pre\text{-}Compton} = (R_{\rm in,km}/D_{10\,\rm kpc})^2 \cos i$, where $R_{\rm in,km}$ is the inner disk radius, $D_{10\,\rm kpc}$ the source distance, and i the disk inclination, by adding the photons Compton scattered (the nthComp component) and those unscattered (the MCD component), assuming that the photons are conserved. We obtained $N_{\rm disk,pre\text{-}Compton} = 0.47^{+0.91}_{-0.23}$. The optical depth of the corona, which is not an explicit parameter of the model but can be derived using Equation (A1) in Zdziarski et al. (1996), is $\sim$22, which is high, similar to that inferred from the MCD+CompTT model. Therefore, we have made the simple assumption that while the optically thick corona can have seed photons from the disk, it does not strongly affect the thermal disk emission in turn in both the MCD+CompTT and MCD+nthComp models.

The other spectra have much lower quality, and we only test the single-component models, i.e., an MCD and a PL. The unfolded spectra are plotted in Figure 3. The *ROSAT*/PSPCB observation R1 can be fitted with either model. We caution that the fit for this observation is limited by the narrow energy band coverage (0.2–2.4 keV) and calibration uncertainty. The *Chandra* observation C2 can also be fitted with either model, but the PL model requires a relatively strong absorption ($N_{\rm H} = 0.24 \times 10^{22}$ cm^{-2}) and a steep PL ($\Gamma_{\rm PL} = 2.9$). Observation C1, the one with (quasi-)periodic flares (Figure 3), can be fitted with

Table 3
Spectral Fit Results

Obs ID	Model	$N_{\rm H}$ (10^{22} cm^{-2})	Other Parameters	$\chi^2_\nu(\nu)$[a]	$L_{\rm abs}$ (10^{38} erg s^{-1})	$L_{\rm unabs}$
(1)	(2)	(3)	(4)	(5)	(6)	
0094360601(X1)	PL	0.06	$\Gamma_{\rm PL} = 2.5$	···	0.22 ± 0.06	0.4 ± 0.1
0094360701(X2)	PL	0.06	$\Gamma_{\rm PL} = 2.5$	···	0.37 ± 0.09	0.6 ± 0.2
0404980101(X3)	PL	$0.15^{+0.01}_{-0.01}$	$\Gamma_{\rm PL} = 2.37^{+0.04}_{-0.04}$, $N_{\rm PL} = 22^{+1}_{-1} \times 10^{-5}$	1.31(560)	$21.5^{+0.5}_{-0.5}$	$42.2^{+2.0}_{-1.9}$
	MCD	$0.01^{+0.01}$	$kT_{\rm MCD} = 0.86^{+0.02}_{-0.02}$, $N_{\rm MCD} = 5.5^{+0.5}_{-0.4} \times 10^{-2}$	1.15(560)	$19.9^{+0.5}_{-0.5}$	$20.6^{+0.5}_{-0.5}$
	MCD+PL	$0.04^{+0.02}_{-0.02}$	$kT_{\rm MCD} = 0.87^{+0.06}_{-0.06}$, $N_{\rm MCD} = 3.6^{+1.2}_{-0.9} \times 10^{-2}$, $\Gamma_{\rm PL} = 2.1^{+0.2}_{-0.2}$, $N_{\rm PL} = 6^{+2}_{-2} \times 10^{-5}$	0.95(558)	$21.2^{+0.6}_{-0.5}$	$25.5^{+2.3}_{-1.8}$
	MCD+nthComp	$0.02^{+0.01}$	$kT_{\rm MCD} = 0.45^{+0.15}_{-0.15}$, $N_{\rm MCD} = 0.23^{+0.16}_{-0.23}$, $\Gamma_{\rm nthComp} = 1.7^{+0.5}_{-0.7}$, $kT_{\rm e,nthComp} = 1.1^{+0.3}_{-0.2}$, $N_{\rm nthComp} = 9^{+7}_{-8} \times 10^{-5}$	0.90(557)	$20.6^{+0.5}_{-0.5}$	$21.5^{+0.7}_{-0.7}$
	MCD+CompTT	$0.01^{+0.01}$	$kT_{\rm MCD} = 0.25^{+0.07}_{-0.04}$, $N_{\rm MCD} = 1.7^{+0.7}_{-0.7}$, $\tau_{\rm compTT} = 11^{+1}_{-1}$, $kT_{\rm e,compTT} = 1.0^{+0.1}_{-0.1}$, $N_{\rm compTT} = 2.8^{+0.6}_{-0.7} \times 10^{-4}$	0.90(557)	$20.6^{+0.5}_{-0.5}$	$21.1^{+0.7}_{-0.5}$
808(C1)	PL	$0.06^{+0.07}$	$\Gamma_{\rm PL} = 2.5^{+0.5}_{-0.4}$, $N_{\rm PL} = 8^{+2}_{-2} \times 10^{-6}$	0.77(10)	$0.9^{+0.2}_{-0.2}$	$1.5^{+0.8}_{-0.3}$
	MCD	$0.01^{+0.02}$	$kT_{\rm MCD} = 0.43^{+0.08}_{-0.06}$, $N_{\rm MCD} = 3.3^{+3.1}_{-1.7} \times 10^{-2}$	1.92(10)	$0.7^{+0.1}_{-0.1}$	$0.7^{+0.1}_{-0.1}$
9553(C2)	MCD	$0.01^{+0.05}$	$kT_{\rm MCD} = 0.68^{+0.10}_{-0.09}$, $N_{\rm MCD} = 2.6^{+2.1}_{-1.0} \times 10^{-2}$	0.71(11)	$3.6^{+0.3}_{-0.5}$	$3.7^{+0.4}_{-0.4}$
	PL	$0.24^{+0.14}_{-0.11}$	$\Gamma_{\rm PL} = 2.9^{+0.5}_{-0.4}$, $N_{\rm PL} = 6^{+3}_{-2} \times 10^{-5}$	0.42(11)	$3.7^{+0.6}_{-0.5}$	$14.4^{+14.0}_{-5.6}$
RP600050N00(R1)	MCD	$0.01^{+0.01}$	$kT_{\rm MCD} = 0.42^{+0.04}_{-0.04}$, $N_{\rm MCD} = 0.46^{+0.21}_{-0.13}$	1.07(16)	$8.3^{+0.5}_{-0.5}$	$8.9^{+0.5}_{-0.5}$
	PL	$0.03^{+0.01}$	$\Gamma_{\rm PL} = 2.1^{+0.2}_{-0.2}$, $N_{\rm PL} = 9.2^{+0.6}_{-0.6} \times 10^{-5}$	1.08(16)	$15.0^{+2.6}_{-1.9}$	$18.3^{+1.6}_{-1.2}$
RH600678N00(R2)	PL	0.06	$\Gamma_{\rm PL} = 2.5$	···	0.2 ± 0.2	0.4 ± 0.4
RH600769N00(R3)	PL	0.06	$\Gamma_{\rm PL} = 2.5$	···	0.0 ± 0.5	0.0 ± 0.8

Notes. The fits were carried out only on observations X3, C1, C2, and R1. The 0.2–10 keV absorbed ($L_{\rm abs}$) and unabsorbed ($L_{\rm unabs}$) luminsosities are given. For observations X1, X2, R2, and R3, they were estimated based on the PL fit to observation C1. The energy bands of the fits are 0.2–10 keV for X3, 0.3–8 keV for C1 and C2, and 0.2–2.4 keV for R1. All errors are at a 90% confidence level.

a PL, but not well with the MCD model (the reduced χ^2 is 1.9). The inferred photon index is $\Gamma_{\rm PL} = 2.5^{+0.5}_{-0.4}$.

We did not carry out spectral fits to the other four observations (R2, R3, X1, and X2) when the source was not significantly detected and subject to strong contamination from bright sources near the nucleus. Instead, we estimated their source luminosities assuming the best-fitting PL model from observation C1, since C1 was the closest in flux to these observations (Table 3). We note that for observations R2 and R3, in which the source was not detected, we calculated the 90% confidence intervals using Bayesian statistics (Kraft et al. 1991).

3.4. The Optical Counterpart

The candidate optical counterpart to ULX2 fortunately appears on the outskirts of a star-forming region devoid of bright sources (Figure 1). `HSTPhot` indicates this counterpart as point-like in all filters. Its VEGA magnitudes are given in Table 2. The counterpart seems relatively red. It was the most significantly detected in the F555W and F814W filters. Further considering that these two filters are less subject to possible emission from accretion activity than the other filters, we used the SYNPHOT package to compare the color of these two filters with the stellar spectra in Pickles (1998), assuming the Galactic extinction of $E(B-V) = 0.02$ (Schlegel et al. 1998). We found that the counterpart has the F555W−F814W color (1.21 mag) the closest to those of G8I (1.09 mag) and K3V (1.16 mag) stars among supergiants and dwarfs in Pickles (1998), respectively. We fitted the F450W, F555W, and F814W fluxes of the counterpart with these two stellar spectra by minimizing the total χ^2, with the normalization of the spectra as a free parameter. The corresponding apparent magnitudes of the best-fitting spectra are listed in Table 2. The fit residuals are $\lesssim$0.1 mag in these filters. In the $H\alpha$ filter F656N, the deviation is slightly larger, with our source brighter than the fits by 0.3–0.4 mag (2σ–3σ). In the UV filter F336W, the excess is much larger, by 1.5 and 0.7 mag compared with the fits with a G8I star and a K3V star, respectively, though in this filter the source was detected only at 6σ. The apparent visual magnitude of our source is $V = 22.22$, corresponding to an absolute magnitude of -6.4 at the distance of M94, which is close to that expected for a G8I star or that for a red globular cluster containing $\sim 2 \times 10^5$ K3V stars. In the above, we have neglected the possible effect of binary evolution on the color of the donor star.

4. DISCUSSION

4.1. ULX2 as a Super-Eddington Accreting Stellar-mass BHB

ULX2 was fortunately captured at different flux levels, showing clear spectral evolution. With similar spectral models tested, we can easily compare ULX2 with the second ULX in M31 (XMMU J004243.6+412519) studied by Middleton et al. (2013). The brightest observation X3 of ULX2 is very similar to the brightest *XMM-Newton* observations XMM3 and XMM4 of XMMU J004243.6+412519. All these observations have $L_{\rm X} \sim 10^{39}$ erg s^{-1} and are better fitted by the MCD+CompTT model than by a PL, an MCD, or their combination. The fits with the MCD+CompTT model to these observations all inferred a relatively cool (<1 keV, which was not well constrained) disk and Comptonization in a cool ($\sim$1 keV) optically thick ($\tau \sim 10$) corona. XMMU J004243.6+412519 is probably a stellar-mass BHB with $M_{\rm BH} \sim 10\,M_\odot$, based on the joint radio/X-ray behavior and the observation of a disk-dominated state at a very low luminosity, supporting that the above spectra are probably characteristic of accretion at the Eddington limit (Middleton et al. 2013). Then ULX2 could be a stellar-mass BHB as well, with an accretion rate around the Eddington limit in observation X3. Many low-luminosity ULXs show similar spectra and could also be explained as supercritically accreting stellar-mass BHBs (Middleton et al. 2013).

If ULX2 is really a stellar-mass BHB, we would expect it to behave similarly to typical Galactic BHBs when it is at well sub-Eddington luminosities. In the fainter observation C2 ($L_{\rm X} \sim 3.6 \times 10^{38}$ erg s^{-1}), the spectrum is softer than observation X3 and can be described with a standard thermal accretion disk, thus consistent with being in the thermal state of Galactic BHBs. The thermal state in Galactic BHBs tends to occur above $\sim$3% of the Eddington limit (Dunn et al. 2010). Assuming observation C2 to be in this state and using its 0.2–10 keV unabsorbed luminosity from the MCD model, we constrained the mass of the BH in ULX2 to be $\lesssim$100 $M_\odot$, supporting the identification as a stellar-mass BHB. We note that for this observation we cannot rule out a steep PL model with relatively strong absorption from the fit. In the even fainter observation C1 ($L_{\rm X} \sim 9 \times 10^{37}$ erg s^{-1}), the spectrum becomes harder again and can be described with a PL with $\Gamma_{\rm PL} \sim 2.5 \pm 0.5$. Such a photon index is often seen in the steep-PL state of Galactic BHBs, and the source might be in such a state in this observation, but considering its large uncertainty, we cannot rule out the source being in the hard state instead. In any case, we might have observed a state transition often seen in BHBs. We clearly need higher quality data for more detailed comparison.

Therefore, transient/highly variable ULXs like ULX2 and XMMU J004243.6+412519 serve a link between persistent low-luminosity ULXs and classical stellar-mass BHBs. This is reminiscent of the first known transient Z source XTE J1701−462 linking Z and atoll sources, the two main classes of weakly magnetized NS LMXBs (Lin et al. 2009b; Homan et al. 2010). Here we briefly discuss the NS LMXB case to gain some insights into the physics involved in the BHB case. Z sources reach the Eddington limit or above and are mostly persistent with variability factors of only a few, while atolls have luminosities typically less than 50% of the Eddington limit and tend to be transient or highly variable. The proof that Z sources accrete at near or super-Eddington limit and are the same class of object as atolls but at different accretion rates based on XTE J1701−462 is very convincing in several ways (Lin et al. 2009b; Homan et al. 2010). First, Z and atoll sources have well-known distinct timing and spectral properties, and XTE J1701−462 showed Z-source properties at high luminosities and then atoll-source ones during the decay in its 2006–2007 outburst. Second, NS LMXBs have a unique way to infer the Eddington luminosity, i.e., radius expansion Type-1 X-ray bursts, which were detected in XTE J1701−462, and the luminosities when XTE J1701−462 behaved as a Z source were indeed near or above the Eddington luminosity inferred from the bursts (Lin et al. 2009a). Finally, the spectral fitting by Lin et al. (2009b) also gathered some evidence that the Eddington limit was reached in the Z-source stage, especially the result that the disk in the Z-source lower vertex had a relatively constant temperature and an increasing inner disk radius with increasing luminosity, deviating from the $L \propto T^4$ trend observed in the atoll-source stage. The increase in the inner disk radius with luminosity is expected because as the mass accretion rate into the disk increases, the more and more inner part of the disk reaches the local Eddington limit, leading to increasing radial advection flow and/or mass outflow (Ohsuga & Mineshige 2007).

Therefore, studies of NS LMXBs not only demonstrate that near- or super-Eddington accretion is possible but also assure us that objects with different outbursting behaviors and luminosities can belong to the same class and have overall spectral/timing properties mainly determined by the accretion rate. All this supports the possibility that most low-luminosity ULXs are in fact near- or super-Eddington accreting stellar-mass BHBs. Galactic BHBs are known to show many similarities to atolls, such as sub-Eddington luminosity, transient behavior, broadband noise, and possibly also disk spectral evolution (van der Klis 2006; Lin et al. 2007), though there are also some differences, such as hotter thermal spectra and stronger millisecond variability in atolls, which could be reasonably ascribed to emission from the impact of materials onto the NS surface. Then there is a question of whether ULXs that are supercritically accreting stellar-mass BHBs also show some properties observed in Z sources. One possible interesting similarity is their generally small long-term variability. Classical Z sources (Sco X-1, GX 17+2, GX 349+2, GX 340+0, GX 5-1, and Cyg X-2), all with a low-mass companion, are persistent with long-term variation factors of only a few (only two Z sources (XTE J1701−462 and IGR J17480−2446), discovered recently, are transients). Most known ULXs are also persistent. Lin et al. (2012b) found only 15 with a long-term variation factor >10 in their 100 ULXs, which is in contrast with the general transient behavior of Galactic BHBs, especially those with a low-mass companion. This could be because most of these ULXs might have a high-mass companion, but from Z sources we cannot rule out that the long-time activity might be related to high accretion rates. It would also be worthwhile to search for similarity of the disk behavior between ULXs and Z sources. Neilsen et al. (2011) had reported similar disk evolution in the BHB GRS 1915+105 in a very bright state, i.e., the ρ state, to that seen in XTE J1701−462 in the Z-source stage. A lot of work is still needed in the future to establish the possible connection between Z sources and low-luminosity ULXs.

4.2. Cause of Short-term X-Ray Variability

The observations of dips from ULX2 make it one of the dipping sources, which include about 20 Galactic X-ray binaries and a few ULXs, such as the ULX in NGC 55 (Stobbart et al. 2004) and NGC 5408 X-1 (Pasham & Strohmayer 2013; Grisé et al. 2013). Long dips lasting for 10%–30% of the orbital phase are mostly found in NS LMXBs and can be explained as due to absorption by a bulge on the edge of the accretion disk at the point where the gas stream impacts the disk (e.g., White & Swank 1982). Short dips less than a few hundred seconds (thus typically <1% of the orbital period) are commonly observed in two BHBs GRO J1655−40 (with a low-mass companion) and Cyg X-1 (with a supergiant companion). They show orbital phase dependence and could be due to absorption in accretion streams from the companion (Kuulkers et al. 2000; Bałucińska-Church et al. 2000; Feng & Cui 2002). It is not clear whether the dipping ULXs in NGC 55 and NGC 5408 also show orbital phase dependence, but they might have similar origin. Dips in ULX2 are short and are thus probably also due to absorption in accretion streams. The spectrum becomes soft in the dips in observation X3, which could be because a hot component is obscured and/or because the absorbing matter is partially ionized. In terms of the MCD+nthComp model that we used to fit observation X3, the dipping spectrum that we created from this observation could be very roughly accounted for with either complete obscuration of the nthComp component (the reduced χ^2 is 3.7 for seven dof) or with the presence of absorbing matter with a column density of 6.5×10^{23} cm^{-2} and ionization parameter of $\log \xi = 2.9$ (the reduced χ^2 is 4.3 for seven dof, using the absorption model zxipcf in XSPEC). We do not have enough dips to search for periodicity, which could otherwise provide information of the orbital period. In any case, the dips often imply that the system is at a high inclination. Detection of ULXs at high inclinations is important, because it poses a problem to use the beaming effect to explain the ultraluminous nature of these sources.

The possible large (quasi-)periodic X-ray modulations/flares in observation C1 are also a special property of ULX2. Similar modulations were also observed in some ULXs such as CXOU J141312.3−652013 in Circinus (∼7.5 hr; Bauer et al. 2001), M51 X-7 (∼2 hr; Liu et al. 2002), and CXOU J013651.1+154547 in M74 (∼2 hr; Krauss et al. 2005; Liu et al. 2005). The main difference is that ULX2 has $L_X \sim 10^{38}$ erg s^{-1} while those sources have $L_X > 10^{39}$ erg s^{-1} when such large modulations were observed. Various explanations for such modulations were discussed by those studies, including the binary eclipse, modulations of the accretion rate due to some instability, and variability at the base of the jet. Because ULX2 might have a high inclination considering the detection of dips, if the flares are periodic, the binary eclipsing explanation seems plausible, with the ∼7 hr period being the orbital period. The main problem for this explanation is that we found no spectral change accompanying the flux variation. Moreover, such modulations seem to be flux and/or spectral state dependent because they were not seen in the brighter/softer observations. Therefore, the disk or jet instability explanations are favored.

4.3. Nature of the Optical Counterpart

Another interesting aspect of ULX2 is our identification of its point-like red optical counterpart candidate. Some ULXs have been reported to have optical counterpart candidates (e.g., Tao et al. 2011; Gladstone et al. 2013). Most of them appear blue and are probably contaminated by accretion activity, while some have a clear red component like our source, such as IC 342 X-1 (Feng & Kaaret 2008) and M81-ULS1 (Liu & Di Stefano 2008). For M81-ULS1, there is also an extra blue component, which was shown by Liu & Di Stefano (2008) to be probably from disk emission, while the red component could be an asymptotic giant branch star. There is some possible UV excess in ULX2, and the most likely explanation is the disk emission too. We note that our source is highly variable while the *HST* observations are not simultaneous with each other or with X-ray observations. Therefore, one explanation for why the counterpart to ULX2 appears red while those to other ULXs are mostly blue is that the *HST* observations of ULX2 were made when it was not X-ray ultraluminous, though the alternative explanation that ULX2 resides in an old cluster is also possible.

5. CONCLUSIONS

We have shown many intriguing properties of ULX2. It is either a highly variable persistent source or a recurrent transient, with a long-term variation factor of at least ∼100 and a duty cycle of at least ∼70%. In the brightest observation X3, the source exhibited as a member of low-luminosity ULXs, with $L_X \sim 2 \times 10^{39}$ erg s^{-1}, and had a spectrum showing a high-energy cutoff but too hard to be described by thermal emission from a standard accretion disk. Short dips, accompanied by spectral softening, are also clearly seen. In the

fainter observation C2 ($L_X \sim 3.6 \times 10^{38}$ erg s^{-1}), the spectrum became softer and is consistent with thermal emission from a standard accretion disk with $kT_{MCD} \sim 0.7$ keV, supporting it as in the thermal state as seen in Galactic BHBs. In the even fainter observation C1 ($L_X \sim 9 \times 10^{37}$ erg s^{-1}), the spectrum becomes harder again, with $\Gamma_{PL} \sim 2.5 \pm 0.5$, and could be in the steep-PL state or the hard state of Galactic BHBs. In this observation, we also observe possible flares that might indicate ~7 hr periodic X-ray modulations. We also identify a possible point-like optical counterpart, whose colors and luminosity resemble a G8 supergiant or a compact red globular cluster containing $\sim 2 \times 10^5$ K dwarfs except for some possible UV excess. Combining all the above properties, we suggest that ULX2 is a stellar-mass BHB with a supergiant companion or with a dwarf companion residing in a globular cluster. The high variability and large duty cycle of ULX2 make it easy for multiwavelength follow-up, which is important for confirmation of some properties that we report here, such as the state transition and possible periodic behavior at low luminosities, and reveal more properties to further constrain its nature.

We thank the anonymous referee for the helpful comments. This work is supported by NASA Grant NNX10AE15G.

REFERENCES

Bałucińska-Church, M., Church, M. J., Charles, P. A., et al. 2000, MNRAS, 311, 861
Bauer, F. E., Brandt, W. N., Sambruna, R. M., et al. 2001, AJ, 122, 182
Bautz, M. W., Pivovaroff, M., Baganoff, F., et al. 1998, Proc. SPIE, 3444, 210
Berghea, C. T., Weaver, K. A., Colbert, E. J. M., & Roberts, T. P. 2008, ApJ, 687, 471
Colbert, E. J. M., & Mushotzky, R. F. 1999, ApJ, 519, 89
Constantin, A., & Seth, A. C. 2012, AdAst, 2012, 178060
Cui, W., Feldkhun, D., & Braun, R. 1997, ApJ, 477, 693
Dolphin, A. E. 2000, PASP, 112, 1383
Done, C., Gierliński, M., & Kubota, A. 2007, A&ARv, 15, 1
Dunn, R. J. H., Fender, R. P., Körding, E. G., Belloni, T., & Cabanac, C. 2010, MNRAS, 403, 61
Evans, I. N., Primini, F. A., Glotfelty, K. J., et al. 2010, ApJS, 189, 37
Farrell, S. A., Webb, N. A., Barret, D., Godet, O., & Rodrigues, J. M. 2009, Natur, 460, 73
Fender, R. P., Belloni, T. M., & Gallo, E. 2004, MNRAS, 355, 1105
Feng, H., & Kaaret, P. 2008, ApJ, 675, 1067
Feng, H., & Soria, R. 2011, NewAR, 55, 166
Feng, Y. X., & Cui, W. 2002, ApJ, 564, 953
Freeman, P. E., Kashyap, V., Rosner, R., & Lamb, D. Q. 2002, ApJS, 138, 185
Gladstone, J. C., Copperwheat, C., Heinke, C. O., et al. 2013, ApJS, 206, 14
Gladstone, J. C., Roberts, T. P., & Done, C. 2009, MNRAS, 397, 1836
Godet, O., Plazolles, B., Kawaguchi, T., et al. 2012, ApJ, 752, 34
Grisé, F., Kaaret, P., Corbel, S., Cseh, D., & Feng, H. 2013, MNRAS, 433, 1023
Homan, J., van der Klis, M., Fridriksson, J. K., et al. 2010, ApJ, 719, 201
Jansen, F., Lumb, D., Altieri, B., et al. 2001, A&A, 365, L1
Jonker, P. G., Torres, M. A. P., Fabian, A. C., et al. 2010, MNRAS, 407, 645
Kalberla, P. M. W., Burton, W. B., Hartmann, D., et al. 2005, A&A, 440, 775
King, A. R. 2009, MNRAS, 393, L41
King, A. R., Davies, M. B., Ward, M. J., Fabbiano, G., & Elvis, M. 2001, ApJL, 552, L109
Komossa, S., & Schulz, H. 1998, A&A, 339, 345
Kraft, R. P., Burrows, D. N., & Nousek, J. A. 1991, ApJ, 374, 344
Krauss, M. I., Kilgard, R. E., Garcia, M. R., Roberts, T. P., & Prestwich, A. H. 2005, ApJ, 630, 228
Kuulkers, E., in't Zand, J. J. M., Cornelisse, R., et al. 2000, A&A, 358, 993
Lightman, A. P., & Zdziarski, A. A. 1987, ApJ, 319, 643
Lin, D., Altamirano, D., Homan, J., et al. 2009a, ApJ, 699, 60
Lin, D., Carrasco, E. R., Grupe, D., et al. 2011, ApJ, 738, 52
Lin, D., Remillard, R. A., & Homan, J. 2007, ApJ, 667, 1073
Lin, D., Remillard, R. A., & Homan, J. 2009b, ApJ, 696, 1257
Lin, D., Remillard, R. A., Homan, J., & Barret, D. 2012a, ApJ, 756, 34
Lin, D., Webb, N. A., & Barret, D. 2012b, ApJ, 756, 27
Lin, D., Webb, N. A., & Barret, D. 2013a, arXiv:1309.0509
Lin, D., Webb, N. A., & Barret, D. 2013b, ApJ, 766, 29
Liu, J., & Di Stefano, R. 2008, ApJL, 674, L73
Liu, J.-F., Bregman, J. N., Irwin, J., & Seitzer, P. 2002, ApJL, 581, L93
Liu, J.-F., Bregman, J. N., Lloyd-Davies, E., et al. 2005, ApJL, 621, L17
McClintock, J. E., & Remillard, R. A. 2006, in Compact Stellar X-ray Sources, ed. W. Lewin & M. van der Klis (Cambridge: Cambridge Univ. Press), 157
Middleton, M. J., Miller-Jones, J. C. A., Markoff, S., et al. 2013, Natur, 493, 187
Middleton, M. J., Sutton, A. D., Roberts, T. P., Jackson, F. E., & Done, C. 2012, MNRAS, 420, 2969
Neilsen, J., Remillard, R. A., & Lee, J. C. 2011, ApJ, 737, 69
Ohsuga, K., & Mineshige, S. 2007, ApJ, 670, 1283
Okada, K., Dotani, T., Makishima, K., Mitsuda, K., & Mihara, T. 1998, PASJ, 50, 25
Pasham, D. R., & Strohmayer, T. E. 2013, ApJ, 764, 93
Pickles, A. J. 1998, PASP, 110, 863
Poutanen, J., Lipunova, G., Fabrika, S., Butkevich, A. G., & Abolmasov, P. 2007, MNRAS, 377, 1187
Remillard, R. A., & McClintock, J. E. 2006, ARA&A, 44, 49
Rots, A. H., & Budavári, T. 2011, ApJS, 192, 8
Schlegel, D. J., Finkbeiner, D. P., & Davis, M. 1998, ApJ, 500, 525
Servillat, M., Farrell, S. A., Lin, D., et al. 2011, ApJ, 743, 6
Steiner, J. F., Narayan, R., McClintock, J. E., & Ebisawa, K. 2009, PASP, 121, 1279
Stobbart, A.-M., Roberts, T. P., & Warwick, R. S. 2004, MNRAS, 351, 1063
Stobbart, A.-M., Roberts, T. P., & Wilms, J. 2006, MNRAS, 368, 397
Strüder, L., Briel, U., Dennerl, K., et al. 2001, A&A, 365, L18
Sutton, A. D., Roberts, T. P., Walton, D. J., Gladstone, J. C., & Scott, A. E. 2012, MNRAS, 423, 1154
Tao, L., Feng, H., Grisé, F., & Kaaret, P. 2011, ApJ, 737, 81
Titarchuk, L. 1994, ApJ, 434, 570
Tonry, J. L., Dressler, A., Blakeslee, J. P., et al. 2001, ApJ, 546, 681
Truemper, J. 1982, AdSpR, 2, 241
Turner, M. J. L., Abbey, A., Arnaud, M., et al. 2001, A&A, 365, L27
van der Klis, M. 2006, in Compact Stellar X-ray Sources, ed. W. Lewin & M. van der Klis (Cambridge: Cambridge Univ. Press), 39
Watson, M. G., Schröder, A. C., Fyfe, D., et al. 2009, A&A, 493, 339
White, N. E., & Swank, J. H. 1982, ApJL, 253, L61
Zdziarski, A. A., Johnson, W. N., & Magdziarz, P. 1996, MNRAS, 283, 193
Życki, P. T., Done, C., & Smith, D. A. 1999, MNRAS, 309, 561